The lncRNA *Malat1* is trafficked to the cytoplasm as a localized mRNA encoding a small peptide in neurons

Wen Xiao,[1] Reem Halabi,[1] Chia-Ho Lin,[1] Mohammad Nazim,[1] Kyu-Hyeon Yeom,[1] and Douglas L. Black[1,2,3,4]

[1]Department of Microbiology, Immunology, and Molecular Genetics, David Geffen School of Medicine, University of California Los Angeles, Los Angeles, California 90095, USA; [2]Molecular Biology Institute, University of California Los Angeles, Los Angeles, California 90095, USA; [3]Eli and Edythe Broad Center of Regenerative Medicine and Stem Cell Research, University of California Los Angeles, Los Angeles, California 90095, USA; [4]Jonsson Comprehensive Cancer Center, David Geffen School of Medicine, University of California Los Angeles, Los Angeles, California 90095, USA

Synaptic function in neurons is modulated by local translation of mRNAs that are transported to distal portions of axons and dendrites. The metastasis-associated lung adenocarcinoma transcript 1 (*MALAT1*) is broadly expressed across cell types, almost exclusively as a nuclear long noncoding RNA. We found that in differentiating neurons, a portion of *Malat1* RNA redistributes to the cytoplasm. Depletion of *Malat1* using antisense oligonucleotides (ASOs) stimulates the expression of particular pre- and postsynaptic proteins, implicating *Malat1* in their regulation. Neuronal *Malat1* is localized in puncta of both axons and dendrites that costain with Staufen1 protein, similar to neuronal RNA granules formed by locally translated mRNAs. Ribosome profiling of cultured mouse cortical neurons identified ribosome footprints within a 5′ region of *Malat1* containing short open reading frames. The upstream-most reading frame (M1) of the *Malat1* locus was linked to the GFP-coding sequence in mouse embryonic stem cells. When these gene-edited cells were differentiated into glutamatergic neurons, the M1-GFP fusion protein was expressed. Antibody staining for the M1 peptide confirmed its presence in wild-type neurons and showed that M1 expression was enhanced by synaptic stimulation with KCl. Our results indicate that *Malat1* serves as a cytoplasmic coding RNA in the brain that is both modulated by and modulates synaptic function.

[*Keywords*: lncRNA; *Malat1*; RNA localization; micro-ORF; local translation]

Supplemental material is available for this article.

Received January 23, 2024; revised version accepted April 12, 2024.

Long noncoding RNAs (lncRNAs) are RNA molecules longer than ~500 nt that lack extended open reading frames (Ransohoff et al. 2018; Mattick et al. 2023). LncRNAs localized to the nucleus can function in chromatin organization, nuclear architecture, genome stability, transcriptional regulation, and RNA processing (Bergmann and Spector 2014; Böhmdorfer and Wierzbicki 2015; Khanduja et al. 2016; Tang et al. 2017; Ouyang et al. 2022), whereas cytoplasmic lncRNAs play similarly diverse roles in RNA stability, microRNA and protein sequestration, and translational control (Lee et al. 2016; Munschauer et al. 2018; Noh et al. 2018; Karakas and Ozpolat 2021). Despite their noncoding classification, many cytoplasmic lncRNAs have been found to associate with ribosomes and be translated (Ingolia et al. 2014; Ruiz-Orera et al. 2014; Wang et al. 2016; Xing et al. 2021). Short peptides encoded by lncRNA open reading frames (micro-ORFs) were found to have function in mRNA processing, DNA repair, muscle regeneration and development, and cancer progression (Anderson et al. 2015; Nelson et al. 2016; Bi et al. 2017; Huang et al. 2017; Matsumoto et al. 2017; Zhang et al. 2017, 2022). Many new micropeptides were recently identified in human brains, although their roles in neuronal maturation or activity are mostly unknown (Duffy et al. 2022).

Malat1 (metastasis-associated lung adenocarcinoma transcript 1) is an abundant and highly conserved lncRNA expressed in many mammalian cell types. The major *Malat1* transcript (~7 kb in humans and 6.7 kb in mice) lacks introns and a poly(A) tail, unlike a typical mRNA. Instead, the *Malat1* transcript undergoes an unusual 3′ end processing reaction in which it is cleaved by RNase

Corresponding author: dougb@microbio.ucla.edu
Article published online ahead of print. Article and publication date are online at http://www.genesdev.org/cgi/doi/10.1101/gad.351557.124.

© 2024 Xiao et al. This article is distributed exclusively by Cold Spring Harbor Laboratory Press for the first six months after the full-issue publication date (see http://genesdev.cshlp.org/site/misc/terms.xhtml). After six months, it is available under a Creative Commons License (Attribution-NonCommercial 4.0 International), as described at http://creativecommons.org/licenses/by-nc/4.0/.

P to generate a tRNA-like small RNA (mascRNA), which is transported to the cytoplasm (Wilusz et al. 2008, 2012; Brown et al. 2012). The 5′ major portion of the cleaved transcript forms a triple-helical structure at its 3′ end that protects it from degradation. These mature *Malat1* transcripts are enriched in nuclear speckles and have been found to affect splicing, chromatin organization, and transcription (Tripathi et al. 2010; Engreitz et al. 2014; Chen et al. 2017; Miao et al. 2022). In neurons, depletion of *Malat1* was found to reduce expression of synaptic proteins and to reduce neurite outgrowth. These effects were attributed to changes in transcription or miRNA availability mediated by the nuclear *Malat1* RNA (Bernard et al. 2010; Chen et al. 2016; Kim et al. 2018; Xie et al. 2021). However, a recent study identified m^6A-modified *Malat1* RNA at neuronal synapses and reported that *Malat1* depletion impaired fear extinction memory (Madugalle et al. 2023).

In this study, we report that *Malat1* transcripts are exported to the cytoplasm and transported into neuronal processes during neuronal development. Unlike previous observations, we found that depletion of *Malat1* from neurons led to upregulation of pre- and postsynaptic proteins important for neuronal maturation. We demonstrated that *Malat1* colocalizes with the neuronal granule protein Staufen1 in puncta within both axons and dendrites of mature neurons. We further discovered that this neuronal *Malat1* is translated to produce a micropeptide and that expression of this micropeptide is stimulated by synaptic activity. These findings suggest alternative mechanisms for how the *Malat1* RNA can affect neuronal maturation and activity.

Results

A portion of Malat1 *RNA is exported to the cytoplasm in differentiating neurons and transported into neurites*

Malat1 is a well-studied lncRNA enriched in nuclear speckles and largely absent from the cytoplasm across many cell types (Tripathi et al. 2010; Miyagawa et al. 2012; Nakagawa et al. 2012). We previously generated extensive RNA sequencing data from fractionated cellular compartments (Yeom et al. 2021). Total ribosomal RNA (rRNA)-depleted RNA was extracted and sequenced from chromatin, nucleoplasm, and cytoplasm fractions of three mouse cell types—embryonic stem cells (ESCs), neuronal progenitor cells (NPCs), and primary cortical neurons—explanted from embryonic day 15 embryos and differentiated for 5 days in culture. We observed that, in contrast to ESCs and NPCs, cortical neurons displayed abundant *Malat1* RNA in the cytoplasm in addition to that in the nuclear fractions (Fig. 1A). Other nuclear lncRNAs, including *Neat1* (Yeom et al. 2021) and *kcnq1ot1* (Supplemental Fig. S1A), maintained their almost exclusively nuclear expression in all three cell types.

We cultured primary cortical neurons from E16 mice (Fig. 1B) and quantified *Malat1* RNA abundance across neuronal maturation by RT-qPCR (Supplemental Table S1). We found that *Malat1* expression increased fourfold relative to *Gapdh* between 0 days in vitro (DIV0) and DIV17. This roughly paralleled a fivefold increase in the neuronal mRNA *Map2*, although the two transcripts differed in their abundance profiles across time (Fig. 1C).

Cell nuclei are difficult to cleanly isolate from cultured neurons after about DIV5. To confirm the release of *Malat1* into the cytoplasm of mature neurons, we used a digitonin elution assay at various stages of neuronal maturation (Supplemental Fig. S1B) to permeabilize the plasma membrane and selectively release the cytoplasmic components (Niklas et al. 2011; Adam 2016). This material was compared with the remaining cellular material containing both cytoplasmic and nuclear contents. RNA was then extracted from the two fractions and assayed by reverse transcription PCR (RT-PCR) (Supplemental Fig. S1B). Notably, cytoplasmic *Malat1* transcripts were detected at DIV2 and increased at DIV5 and DIV10 (Supplemental Fig. S1B). This was similar to cytoplasmic mRNAs (*Gapdh* and *Actb*) and in contrast to the nuclear RNAs *Neat1* and *U6* that were found almost entirely in the combined nuclear and cytoplasmic fraction at all days in vitro (Supplemental Fig. S1B).

We also analyzed previously published RNA-seq data generated from rat neuronal processes that had extended through a filter to allow the clean separation of cell projections from cell bodies and nuclei (Saini et al. 2019). These data showed that *Malat1* was abundantly expressed in neurites, whereas another nuclear lncRNA, *Neat1*, was absent (Supplemental Fig. S1C,D; Saini et al. 2019).

We next sought to directly observe *Malat1* in neurons and assess its subcellular distribution using single-molecule RNA fluorescence in situ hybridization (smFISH). We designed and labeled 94 fluorescently tagged oligonucleotides that tile the *Malat1* sequence (Xiao et al. 2023). As expected, these probes densely stained the nuclei in neurons throughout maturation (Fig. 1D). In addition, there were many small *Malat1* stained puncta in the neuronal processes whose number increased with maturation (Fig. 1D,E). *Malat1* puncta were observed in both axons and dendrites, with larger numbers in axons, as defined by the cellular morphology (Fig. 1E). Measuring the punctal density of *Malat1* along axons or dendrites, the *Malat1* puncta decreased with distance from the soma (cell body) (Fig. 1F,G). To confirm the specificity of the *Malat1* FISH signal, we split the 94 *Malat1* probes into two subsets targeting either the 5′ or 3′ portion of the *Malat1* transcript. Each 47 probe subset was labeled with a different fluorophore (ATTO565 or ATTO647N) (Supplemental Fig. S2A; Supplemental Table S2). As shown in Supplemental Figure S2, B and C, the two probe subsets colocalized well along the neurites, indicating that they are staining both the 5′ and 3′ portions of the RNA. We also designed FISH probe sets targeting the short and long isoforms of the nuclear long noncoding RNA *Neat1* (Supplemental Fig. S2D; Supplemental Table S2). In contrast to *Malat1*, the two isoforms of *Neat1* both showed only nuclear localization in cultured neurons (Supplemental Fig. S2D). Overall, these results demonstrate that *Malat1* RNA is

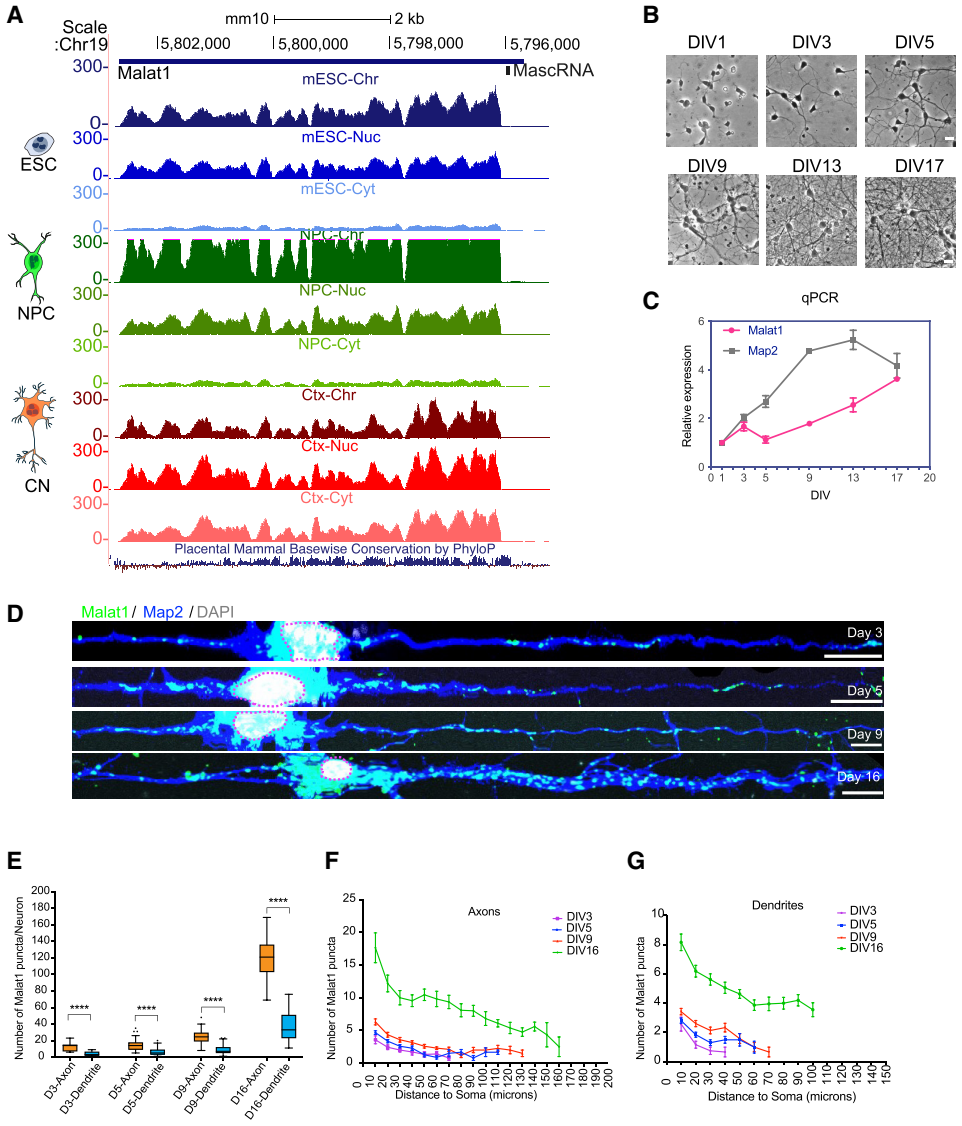

Figure 1. *Malat1* is exported from the nucleus to the cytoplasm during neuronal differentiation. (*A*) Genome browser tracks of the *Malat1* locus displaying RNA-seq reads from chromatin, nucleoplasmic, and cytoplasmic fractions of three cell types—mouse embryonic stem cells (ESCs; blue), neuronal progenitor cells (green), and primary cortical neurons (red)—at 5 days in vitro (DIV5). (*B*) Morphology of cultured primary cortical neurons at different days in vitro used for RNA quantification in *C*. (*C*) RT-qPCR analysis of *Malat1* and *Map2* expression in the cells shown in *B*. (*D*) *Malat1* RNA fluorescence in situ hybridization (FISH; green) combined with Map2 protein staining (blue) in neurons at different stages of development. Scale bar, 10 µm. (*E*) Quantification of *Malat1* FISH puncta in axons and neurites. (*F*,*G*) *Malat1* spot counts along axons and dendrites are shown with distance from the cell body (soma) at different days in vitro. (****) $P < 0.0001$.

transported from the nucleus to the cytoplasm in developing cortical neurons and is trafficked into neurites away from the soma.

Depletion of Malat1 *stimulates the expression of synaptic proteins*

Previous studies found that *Malat1* depletion by antisense oligonucleotides (ASOs) decreased the levels of synapsin and other synaptic markers in cultured hippocampal neurons, whereas *Malat1* overexpression led to increases in synapse density (Bernard et al. 2010; Madugalle et al. 2023). These effects were thought to result from the loss of nuclear *Malat1*, but given the observations above, they could also result from effects of cytoplasmic *Malat1*. To examine the effects of *Malat1* in our system, we designed three GapmeR oligonucleotides (ASO-a, ASO-b, and ASO-c) complementary to sequences in *Malat1* that target the RNA for degradation by RNase H (Supplemental Fig. S2E). Each of these ASOs induced efficient (>90%) depletion of *Malat1* as measured by RT-qPCR (Supplemental Fig. S2F; Supplemental Table S1) and eliminated *Malat1* staining by FISH (Supplemental Fig. S2G). To examine the effects of *Malat1* depletion in our cortical

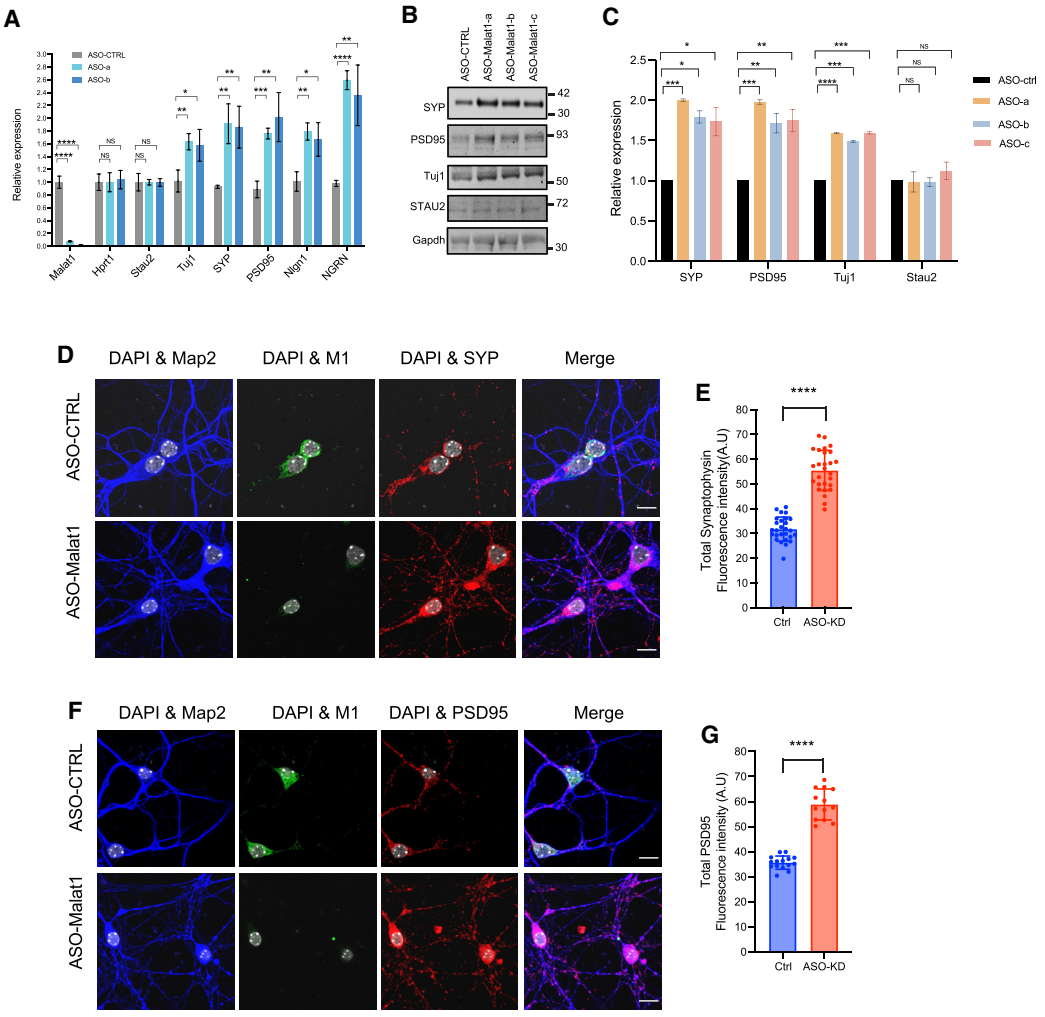

Figure 2. *Malat1* knockdown stimulates expression of pre- and postsynaptic proteins. (*A*) qPCR analysis of RNA levels for selected genes after *Malat1* knockdown compared with control (Ctrl) ASO treatment. (*B*) Immunoblot analysis of *SYP*, *PSD95*, *Tuj1*, *Stau2*, and *Gapdh* proteins after *Malat1* knockdown. Immunofluorescent secondary antibodies were used to detect and quantify each protein signal. (*C*) Quantification of immunoblot bands in *B* measured relative to Gapdh. (*D*) Immunofluorescence of Synaptophysin and M1 peptide before and after *Malat1* depletion by ASOs. (*E*) Quantification of total Synaptophysin fluorescence intensity in control (Ctrl) and *Malat1* knockdown (KD) neurons. (*F*) Immunofluorescence of PSD95 and M1 peptide after *Malat1* depletion by ASOs. (*G*) Quantification of mean PSD95 intensity in control and *Malat1* knockdown neurons. (*) $P \leq 0.05$, (**) $P \leq 0.01$, (***) $P \leq 0.001$, (****) $P < 0.0001$, (NS) nonsignificant ($P > 0.05$).

cultures, we treated the cells with GapmeR ASOs and then assayed a variety of neuronal and synaptic markers by RT-qPCR and immunoblot. We observed increased mRNA levels for some synaptic proteins such as Synaptophysin and NRGN and for the neuronal β-tubulin protein Tuj1 (Fig. 2A). The magnitude of these mRNA changes varied depending on the protein, with the largest being about twofold for NRGN. Synaptophysin and PSD95 proteins also increased about twofold upon *Malat1* depletion, as measured by immunoblot (Fig. 2B,C). This was confirmed by immunofluorescence, where both the presynaptic synaptophysin and postsynaptic PSD95 were seen to increase in the soma and throughout the dendritic arbor after GapmeR treatment (Fig. 2D–G). Thus, in our system, *Malat1* acts to reduce the expression of certain neuronal proteins. It was previously reported that partial knockdown of *Malat1* in cultured hippocampal neurons led to reduced numbers of Synapsin 1-positive synaptic boutons and reduced expression of mRNAs for certain synaptic components (Bernard et al. 2010). We also found that depletion of *Malat1* produced a 20%–40% decrease of Synapsin 1 protein as measured by immunoblot and immunofluorescence (Supplemental Fig. S2H–M). *Malat1* thus appears to modulate synaptic components both positively and negatively.

Malat1 *colocalizes with Staufen1 in neuronal mRNA granules*

Many neuronal mRNAs are packaged into mRNP granules for their transport into distal processes in which they are locally translated (Knowles et al. 1996; Holt

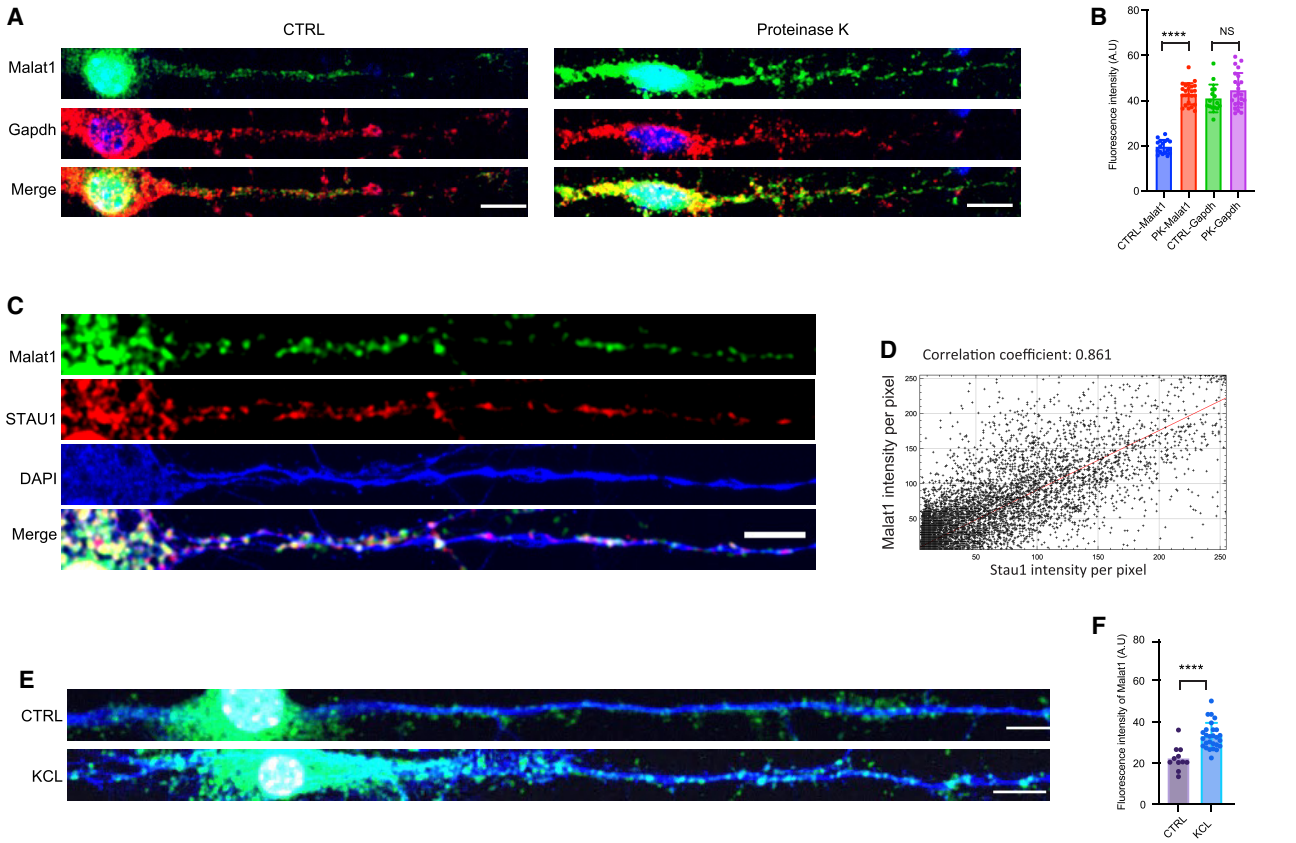

Figure 3. *Malat1* RNA is masked by protein in the cytoplasm and costains with Staufen1. (*A*, *left*) *Malat1* (green) and Gapdh (red) RNA FISH in control primary neurons at DIV13. (*Right*) *Malat1* (green) and *Gapdh* (red) RNA FISH in neurons treated with limited proteinase K (see the Materials and Methods). (*B*) Quantification of the mean fluorescent intensity in cells shown in *A*. Twenty-five cells were measured for each probe and condition. (*C*) *Malat1* RNA FISH combined with Map2 and STAU1 protein staining in cultured cortical neurons at DIV13. (*D*) Pixel intensity correlation of the Stau1 and *Malat1* signals. (*E*) RNA FISH of *Malat1* (green) in control primary neurons (H_2O) and neurons exposed to 100 mM KCl for 60 min, with fixation 10 min later. (Blue) Map2 protein stain. (*F*) Mean fluorescent intensity quantification for 20 cells of each condition in *E*. Scale bar, 10 μm.

et al. 2019; Grzejda et al. 2022; Bauer et al. 2023). The mRNAs in these particles are densely packaged with proteins and have been observed to have low accessibility to FISH probes (Fritzsche et al. 2013; Bauer et al. 2023). Limited proteinase treatment has been used to expose these RNAs and boost their FISH signals (Buxbaum et al. 2014; Young et al. 2020; Sato et al. 2022). Similar to the previous observations, we found that *Malat1* puncta in the cytoplasm became brighter and more numerous after limited proteinase K treatment (Fig. 3A,B). In contrast, the FISH signal for the actively translated *Gapdh* mRNA was not altered by the protease treatment (Fig. 3A,B).

Two proteins that associate with mRNA in neuronal granules are Staufen1 and Staufen2 (Mallardo et al. 2003; Kiebler and Bassell 2006). To examine Staufen1 association with *Malat1*, we combined smFISH and immunofluorescence (IF) using the *Malat1* hybridization probes and an antibody against Staufen1. We found that *Malat1* and Staufen1 were strongly but not completely colocalized in the cytoplasm of neurons at DIV16 (Fig. 3C,D). The staining of Staufen2 protein was also strongly correlated with the *Malat1* FISH signal (Supplemental Fig. S3A,B). To assess possible direct interactions of *Malat1* RNA with Staufen proteins, we examined a published iCLIP data set for Staufen2 in mouse brains (Sharangdhar et al. 2017). These data exhibit extensive significant cross-linking sites for Staufen2 across the *Malat1* transcript (Supplemental Fig. S3I). The specificity of the cross-linking is confirmed by peaks in the 3′ UTR of *CaMK2a*, a known binding region, and the absence of cross-linking seen in *Neat1* (Supplemental Fig. S3J,K). *CaMK2a* mRNA is a well-characterized localized mRNA known to form granules. FISH analysis of *CaMK2a* mRNA yielded the expected pattern of punctal staining in dendrites. These puncta showed minimal overlap with *Malat1*, indicating that the two RNAs are in different granules (Supplemental Fig. S3C,D). Neuronal mRNA granules are trafficked along neuronal processes but are excluded from synaptic spines (Kiebler and Bassell 2006; Batish et al. 2012). Costaining for the pre- and postsynaptic proteins Synaptophysin and PSD95 with *Malat1* RNA revealed that *Malat1* was not colocalized with glutamatergic synapses (Supplemental Fig. S3E–H). Thus, the

Malat1 in neuronal processes is packaged with Staufen proteins into structures similar to mRNA granules.

Neuronal mRNAs traveling within dendrites can be mobilized for translation by synaptic stimulation, which induces their local unpackaging from the granule and increases their FISH signal (Schuman 1999; Krichevsky and Kosik 2001; Kiebler and Bassell 2006; Buxbaum et al. 2014; Holt et al. 2019; Formicola et al. 2021). Similarly, we found that depolarization of the cultured neurons with 60 mM KCl for 1 h led to a significant increase in the cytoplasmic FISH staining for *Malat1* (Fig. 3E,F). This increased signal was not due to an increase in *Malat1* RNA abundance as measured by RT-PCR (Supplemental Fig. S2N–P). Taken together these data indicate that cytoplasmic *Malat1* is localized to RNA granules in neuronal processes and is released in an activity-dependent manner.

Small polypeptides are encoded within the 5′ region of Malat1

Many RNAs originally classified as noncoding have been found to encode small peptides serving a variety of cellular functions (Nelson et al. 2016; Huang et al. 2017; Matsumoto et al. 2017). The activity-dependent release of cytoplasmic *Malat1* from mRNA granules in neurons raised the possibility that *Malat1* might engage with ribosomes and be translated. To assess this, we examined ribosome profiling data of mRNAs in cultured cortical neurons. We identified several ribosome peaks within the 5′ region of *Malat1*, suggesting that *Malat1* associates with ribosomes (Fig. 4A). This was in contrast to two other lncRNAs, *Neat1* and *Norad*, that showed no ribosomal binding peaks (Supplemental Fig. S4B,C). Re-examining previously reported ribosome profiling data for dendritically localized mRNAs in rat neurons showed peaks similar to those of mouse *Malat1* (Saini et al. 2019). Similar peaks were also previously observed in human *Malat1* from HeLa cells (Wilusz et al. 2012). For typical neuronal mRNAs such as *Map2* (Supplemental Fig. S4A), ribosome occupancy was limited to the open reading frames. Searching for possible ORFs near the ribosomal peaks within *Malat1*, we identified six potential short ORFs (M1–M6), each with an ATG start codon and a minimal ORF length of 30 nt (Fig. 4A). These ORFs exhibited relatively modest but statistically significant conservation between mammalian species (Fig. 4B; Supplemental Fig. S5A,B). Of these ORFs, only M1 showed overlapping ribosome binding, and this did not extend equally throughout the ORF. Similar incomplete coverage has been observed in other short ORFs (Brar et al. 2012; Powers et al. 2022). This ribosome association with *Malat1* could result in productive translation, serve some regulatory role, or simply be adventitious.

To determine whether the *Malat1* ORFs are translated in neurons, we created fusion constructs containing the EGFP ORF, minus its own ATG, linked as an in-frame C-terminal extension of each *Malat1* ORF (Supplemental Fig. S6A). Transient expression of these constructs in N2a neuroblastoma cells and assay by fluorescence microscopy revealed that the M1 and M5 ORFs can initiate productive translation to produce the fused GFP (Supplemental Fig. S6B). Immunoblots confirmed that these proteins migrated at the expected masses of the M1 and M5 fusion proteins (Supplemental Fig. S6C). Notably, GFP expression was lost when the M1 start codon was mutated from ATG to TAG, indicating that initiation is occurring at the M1 ATG (Supplemental Fig. S6A–C). To confirm that GFP was translated from the entire *Malat1* and not a fragment of the ectopically expressed RNA, we performed RNA FISH in N2a cells after transient expression of the M1-GFP and M1-mut-GFP constructs (Supplemental Fig. S6D). *Malat1* FISH signals were observed in both rhw nucleus and cytoplasm (Supplemental Fig. S6D). The cytoplasmic signal for *Malat1* colocalized with the FISH signal for GFP, indicating that the GFP protein was translated from the full-length *Malat1*. The M1-mut-GFP *Malat1* transcripts were localized to the cytoplasm but did not produce GFP protein (Supplemental Fig. S6D). These results demonstrate that the M1 ORF is translated from the whole *Malat1* transcript when expressed from a plasmid.

The M1 peptide is translated from RNA produced from the endogenous Malat1 *loci*

To confirm that the M1 peptide is produced from endogenous *Malat1*, we used CRISPR–Cas9 editing of the *Malat1* locus in mouse embryonic stem cells (ESCs; embyronic day 14 [E14]) to insert GFP as a C-terminal extension of the M1 ORF. This generated a knock-in GFP-tagged M1 ORF (M1-WT-KI) (Fig. 4C). As a negative control, a parallel construct replaced the M1 ATG start codon with TAG to create a mutant knock-in allele of the M1 ORF (M1-mut-KI) (Fig. 4C). Genotyping individual edited clones identified one homozygous and four heterozygous M1-WT-KI lines, as well as three heterozygous M1-mut-KI lines (Supplemental Fig. S7A,B). The correct in-frame insertion of GFP into the *Malat1* loci was confirmed by Sanger sequencing (Supplemental Fig. S7C). Neither the M1-WT-KI nor the M1-mut-KI alleles exhibited GFP fluorescence in ESCs, as expected from the nuclear localization of *Malat1* (Fig. 4D). We then differentiated the wild-type and GFP knock-in ESC lines into glutamatergic neurons (Supplemental Fig. S7D). All three lines differentiated efficiently into cells with neuronal morphology that expressed neuronal markers Tuj1, PSD95, and vGlut1, as assayed by RT-PCR and immunofluorescence (Supplemental Fig. S7E–G). We found that GFP protein was expressed in the M1-WT-KI neurons but was absent in the M1-mut-KI neurons, indicating translation of the endogenous *Malat1* M1 ORF in differentiated neurons (Fig. 4E). The M1-GFP expression was selective to neurons and absent from nonneuronal cells in the culture. The expression of M1-GFP protein was also validated by immunoblot using GFP and M1 antibodies (described below) in the ESC-derived neurons (Fig. 4F). These data demonstrate that in neurons, but not in ESCs, *Malat1* RNA undergoes translation initiation at the start codon of the M1 ORF.

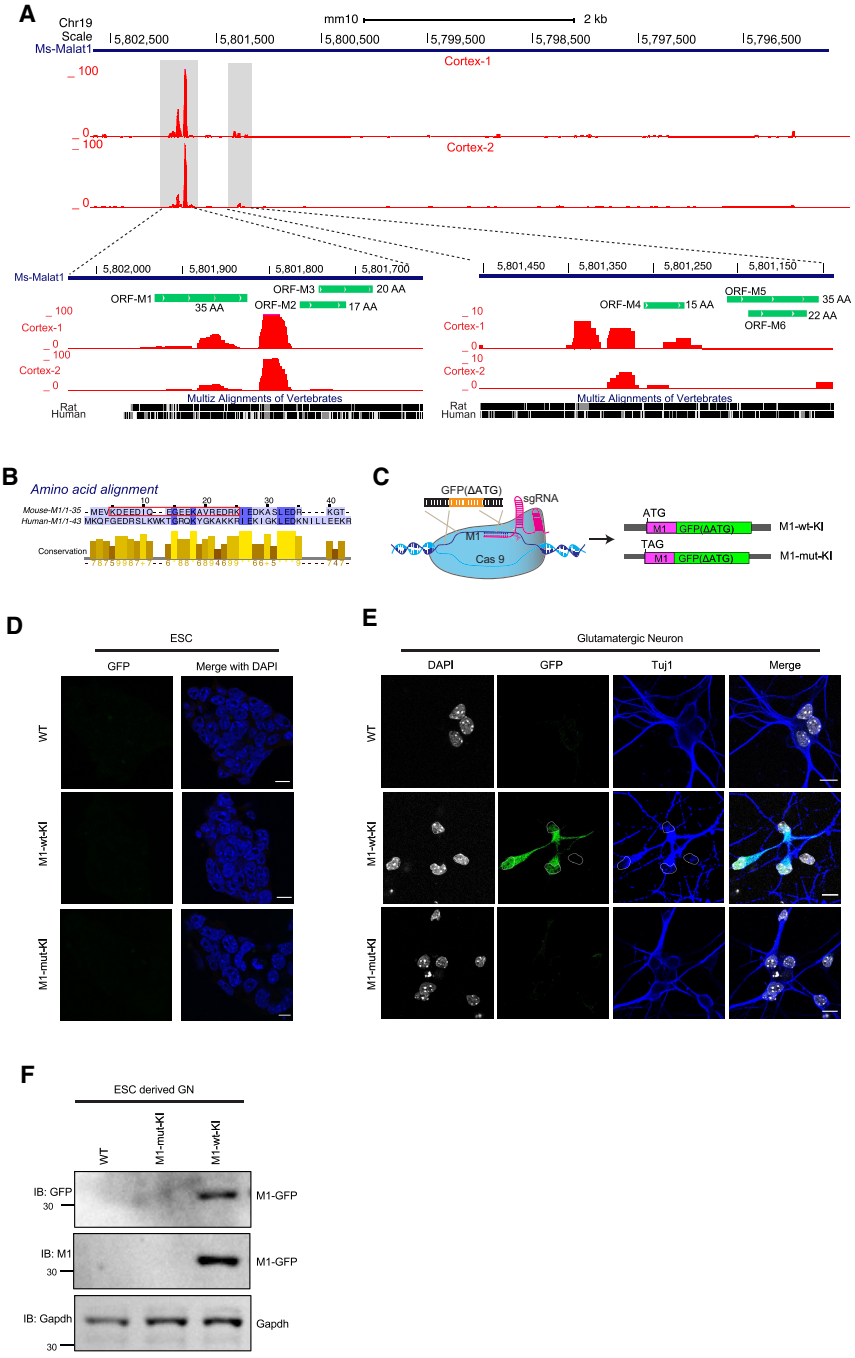

Figure 4. *Malat1* is bound by ribosomes and translated in neurons. (*A*, *top*) Genome browser view of the *Malat1* locus displaying ribosome profiling data in cultured cortical neurons. (*Bottom*) Enlarged views of the gray-highlighted ribosome binding peaks. Potential ORFs are shown as green bars with their peptide lengths. (*B*) Amino acid alignment of the mouse and human M1 peptides by ClustalW. The red box highlights the peptide sequence used as an antigen to raise antibodies to the M1 protein. (*C*) Diagram of CRISPR–Cas9 targeting to knock in the GFP-coding sequence as a C-terminal fusion with M1 at the endogenous *Malat1* loci of embryonic stem cells. M1-WT-KI contains the M1 ATG initiation codon, and M1-mut-KI has this codon mutated to TAG. (*D*) Fluorescent images of parental and genome-edited ESCs showing a lack of GFP fluorescence in all three genotypes. (*E*) GFP fluorescence of WT and genome-edited cells after differentiation into glutamatergic neurons. The knock-in cells containing the M1 initiation codon are now expressing GFP. (*F*) Immunoblot analysis of M1-GFP in glutamatergic neurons derived from engineered ESC lines probed with GFP and M1 antibodies.

M1 peptide expression is enhanced by depolarization

To assay the presence of the M1 peptide without a GFP fusion, we raised an antibody to a 19 amino acid segment of the 35 residue peptide (Fig. 4B). We confirmed the reactivity and specificity of the antibody in immunoblot assays in N2a cells expressing an RFP-M1 fusion protein (Supplemental Fig. S8A,B). The M1 antibody also immunoprecipitated the GFP-M1 fusion protein (Supplemental Fig. S8B, C). In immunofluorescence assays of N2a cells expressing RFP fusion proteins, the antibody yielded abundant cytoplasmic staining in cells expressing RFP-M1 and no signal in cells expressing RFP fused to the M6 peptide or to the Rbfox1 protein (Supplemental Fig. S8D,E). These experiments confirmed that the M1 antibody could detect the protein with minimal background. The short length of the native M1 peptide precluded its detection by immunoblot.

Immunofluorescent staining of cultured neurons with the M1 antibody detected expression of the native protein in the cytoplasm and dendritic processes (Fig. 5A). To confirm that the fluorescent staining was derived from the M1 peptide and not another reactivity of the antibody, we treated the neurons with the GapmeR oligos to

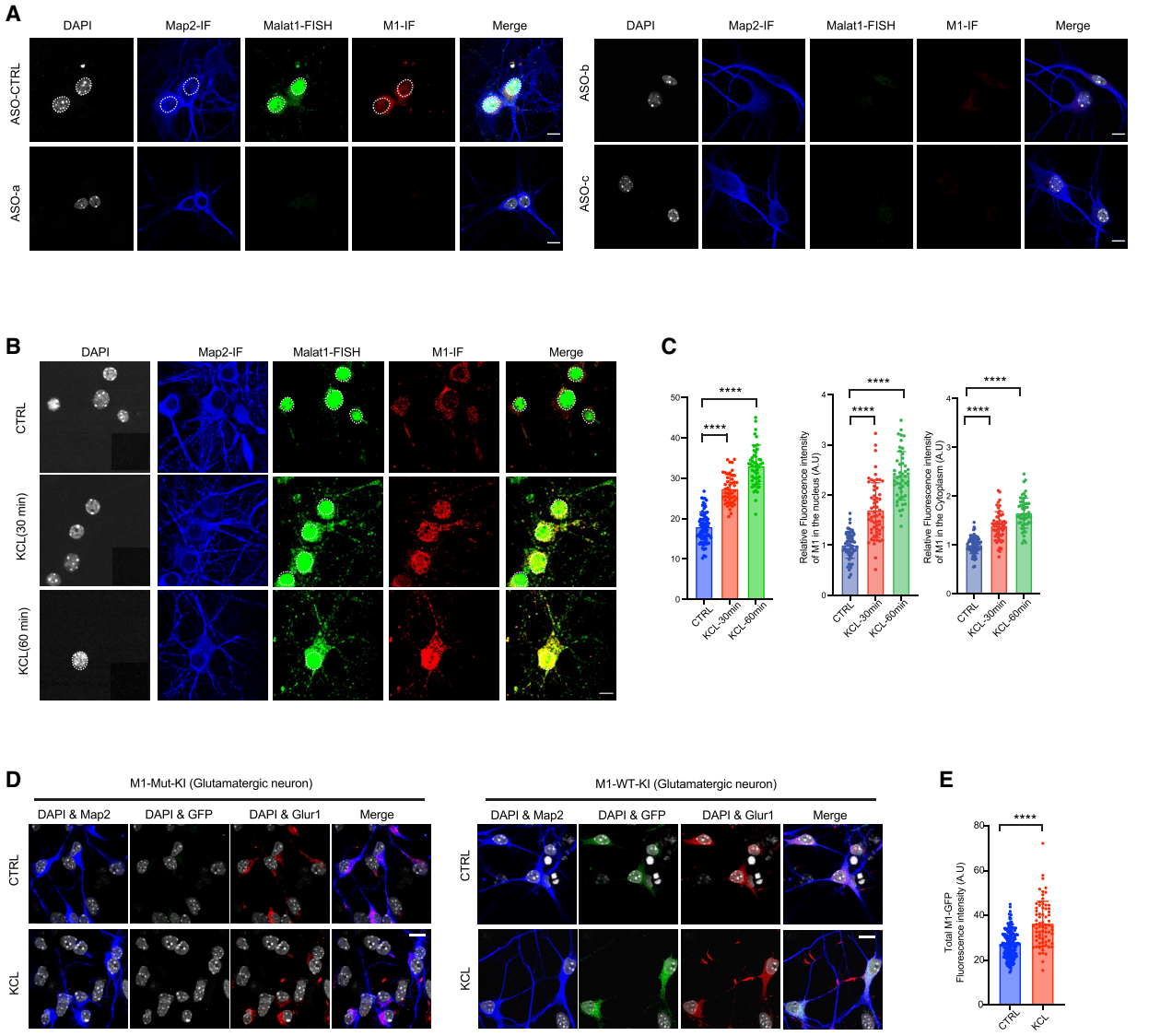

Figure 5. The M1 peptide is detected in primary neurons and is upregulated by membrane depolarization. (*A*) M1 peptide immunofluorescence before and after *Malat1* knockdown by ASOs in primary neurons. (*B*) Antibody staining of the endogenous M1 peptide after KCl treatment for 30 or 60 min in primary cortical neurons. (*C*, *left*) Quantification of mean IF intensities of 50 neuronal cells from *B*. (*Middle*) Relative mean fluorescence intensity of nuclear M1. (*Right*) Relative mean fluorescence intensity of cytoplasmic M1. (*D*) Immunofluorescence of Map2, M1-GFP, and GluR1 in glutamatergic neurons derived from M1-WT-KI and M1-mut-KI ESC lines. GFP indicates signal for endogenous M1-GFP. Anti-Glur1 was used as a marker for glutamatergic neurons. (*E*) Quantification of mean fluorescent intensities for >50 cells from *D*. (****) $P < 0.0001$. Scale bar, 10 µm.

degrade *Malat1* (Supplemental Fig. S2D). Importantly, depletion of Malat1 eliminated the immunofluorescence staining by the M1 antibody (Fig. 5A). Thus, endogenous M1 peptide encoded by *Malat1* is produced in cultured neurons.

We showed above that KCl depolarization resulted in increased *Malat1* FISH signal in neurons without an increase in Malat1 abundance, presumably due to unpackaging of the RNA from neuronal granules (Fig. 3E,F; Krichevsky and Kosik 2001; Bi et al. 2006; Buxbaum et al. 2014; Mofatteh 2020; Formicola et al. 2021). To test whether this activity-dependent release of local *Malat1* transcripts resulted in increased M1 micropeptide translation, we depolarized primary cortical neurons with 60 mM KCl (Ueda et al. 2022). We found that KCl depolarization for 30 and 60 min led to 1.5-fold and twofold increases, respectively, in M1 staining over the whole cell. The nuclear M1 protein was notably increased, indicating that the small M1 peptide can enter the nucleus after synthesis (Fig. 5C). We also examined expression of M1-GFP in the ESC-derived neurons. In these cells, GFP fluorescence increased 35% after KCl treatment (Fig. 5D,E). Overall, these data indicate that neurons translate *Malat1* RNA to produce the M1 peptide and that M1 peptide expression is increased with neuronal activity.

Blocking synthesis of the M1 peptide partially recapitulates depletion of Malat1 *RNA*

To examine the contribution of the M1 peptide to the effects of *Malat1* loss, we specifically blocked its translation with antisense oligonucleotides. 2′MOE-modified ASOs were designed to hybridize to the M1 initiation codon or the initial segment of the GFP reading frame (Fig. 6A). To confirm the effects of these ASOs on protein expression, they were cotransfected with the M1-GFP plasmid into 293T cells. Both ASO-block-M1 and ASO-block-GFP significantly reduced expression of the M1-GFP fusion protein as seen by immunoblot and GFP fluorescence, whereas a control ASO (ASO-Ctrl) had no effect (Fig. 6B,C). We then applied the ASO-block-M1 and ASO-Ctrl oligos to primary cultured cortical neurons (Fig. 6D). Immunofluorescence confirmed the inhibition of M1 protein expression by ASO-block-M1 (Fig. 6H). Depletion of the M1 peptide by ASO-block-M1 led to significant increases in Synaptophysin (~1.5-fold) and PSD95 (~1.2-fold) proteins as measured by immunoblot and immunofluorescence (Fig. 6D–I). Although the effects were more modest than the full knockdown, loss of the M1 peptide alone recapitulated the effects of *Malat1* knockdown, indicating that at least a portion of *Malat1* activity in affecting neuronal gene expression stems from its M1 peptide gene product.

Discussion

Malat1 *is exported to the cytoplasm in neurons*

We demonstrated that in postmitotic neurons a portion of the typically nuclear lncRNA *Malat1* is exported into the cytoplasm, where it is translated to produce a micropeptide (M1). The unusual processing pathway of *Malat1* and its lack of a poly(A) tail do not preclude its translation (Wilusz et al. 2008, 2012; Brown et al. 2012). The 3′ portion of the *Malat1* RNA was previously shown to enhance translation of an upstream ORF when present in a reporter mRNA (Wilusz et al. 2012).

Malat1 has also been found in the cytoplasm of several types of cancer cells, including bladder, hepatic, and breast cancer, and in the cytoplasm of platelet precursor cells (Shih et al. 2021; Zhao et al. 2021; Sun et al. 2023; Zhu et al. 2023). It is not clear whether *Malat1* RNA is translated in these cells, but it was found to encode an antigenic peptide in colorectal cancer cells (Barczak et al. 2023). The mechanisms that allow selective release of *Malat1* from the nucleus are not clear. *Malat1* is normally sequestered on chromatin through a mechanism that requires binding by the U1 snRNP (Yin et al. 2020). In addition to splicing, U1 also functions to suppress premature polyadenylation during transcription (Venters et al. 2019). Interestingly, changes in U1 activity both after neuronal stimulation and in cancer cells are thought to cause

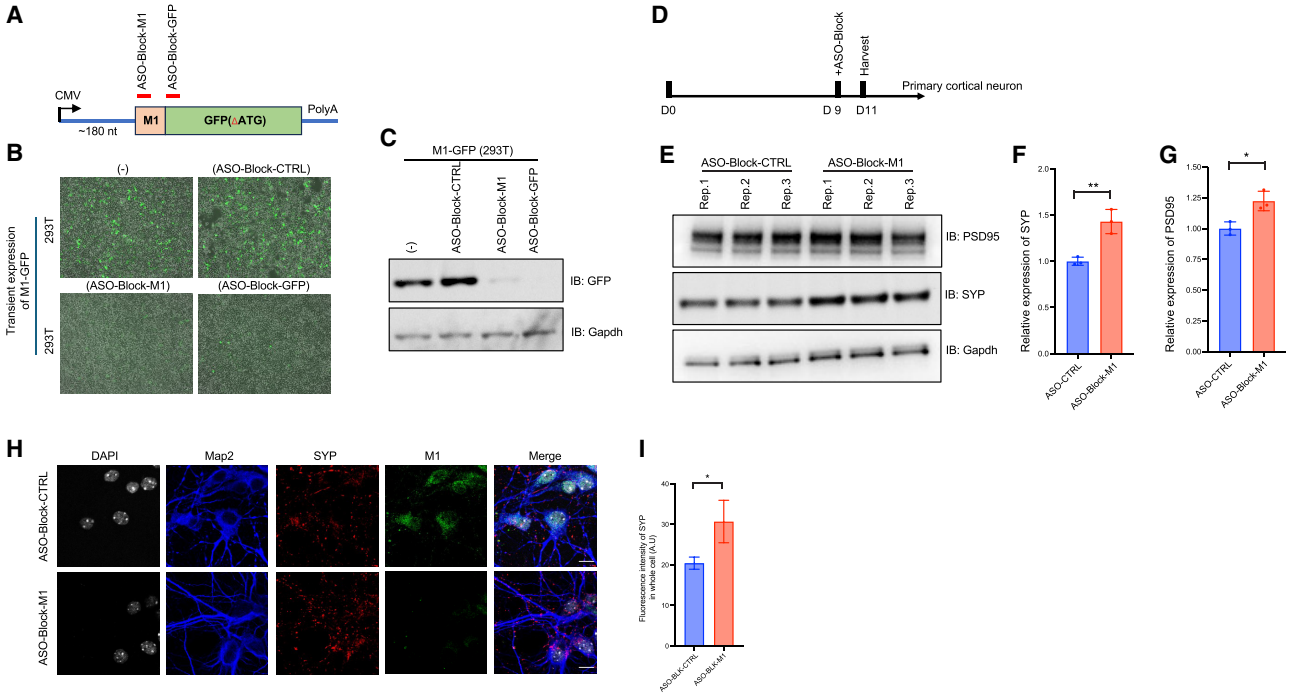

Figure 6. Inhibition of M1 peptide translation increases expression of Synaptophysin and PSD95 proteins. (*A*) Diagram of the M1-GFP construct showing the location of blocking ASOs. (*B*) GFP fluorescence in 293T cells cotransfected M1-GFP plasmid and blocking ASOs. (*C*) Immunoblot of cell lysates from *B* probed for GFP and Gapdh proteins. (*D*) Time line of ASO treatment. (*E*) Immunoblot of SYP and PSD95 in ASO-block-Ctrl- and ASO-block-M1-treated primary neurons. (*F*,*G*) Quantification of band intensities from *E*. (*H*) Immunofluorescence of Synaptophysin and M1 peptide before and after M1 blockage by ASOs. (*I*) Quantification of Synaptophysin whole-cell fluorescence intensity from *H*.

the global activation of new cleavage and polyadenylation sites (Berg et al. 2012). Thus, the release of *Malat1* for nuclear export selectively in neurons may involve reduced activity or availability of U1 in these cells. However, U1 inhibition was found to release *Malat1* from chromatin into the soluble nucleoplasm but not release its export to the cytoplasm. Thus, changes in U1 function alone are unlikely to be sufficient for *Malat1* export. *Malat1* enrichment in nuclear speckles also requires multiple RNA binding proteins (Miyagawa et al. 2012; Wang et al. 2019). Inhibition of U1 or depletion of the nuclear speckle factors do not release Malat1 into the cytoplasm. Additional factors mediating its nuclear localization could include an expression and nuclear retention element (ENE) similar to those found on viral noncoding RNAs (Conrad and Steitz 2005; Brown et al. 2012) and/or m^6A modifications seen in synaptically localized *Malat1* (Madugalle et al. 2023).

Malat1 *is a localized mRNA*

We found that *Malat1* is packaged into neuronal granules that contain Staufen protein and are trafficked into neuronal processes of developing cortical neurons. *Malat1* has been observed in neurites of hippocampal neurons by expansion microscopy (Alon et al. 2021) and was found to enrich in synaptic fractions after a fear extinction learning protocol (Madugalle et al. 2023). Dendritic RNA granules contain mRNAs that are translationally silent and masked to detection by FISH (Buxbaum et al. 2014; Bauer et al. 2023). They are transported along processes through association with microtubule-based motors to allow their selective unpackaging and translational activation at specific stimulated synapses (Fritzsche et al. 2013; Holt et al. 2019). Similar to localized mRNA, both protease treatment and depolarization with KCl dramatically increase the detection of neuritic *Malat1* by FISH. Neuronal depolarization with KCl also increases synthesis of the *Malat1*-encoded M1 peptide. These data together uncover a new function for *Malat1* as not only a nuclear lncRNA but also a cytoplasmic coding RNA.

Functions of Malat1 *translation products*

We found that the peptide encoded by the M1 ORF is expressed from the endogenous *Malat1* locus in stimulated neurons. So far, the M1 peptide is the only *Malat1* translation product directly observed in neurons. We did observe modest translation of an M5 ORF-GFP fusion produced from a transgene in N2a cells. Peptides from additional *Malat1* ORFs may be synthesized in other cells or conditions. Further work interrogating the function of M1 and perhaps other peptides should shed light on the roles of micropeptides in neuronal maturation (Duffy et al. 2022).

The existence of cytoplasmic, translated *Malat1* must now be considered in interpreting the effects of *Malat1* depletion experiments. An earlier study found that loss of *Malat1* reduced expression of certain synaptic proteins in hippocampal neurons (Bernard et al. 2010). Others found that Malat1 knockdown in N2a cells or hippocampal neurons inhibited neurite outgrowth (Chen et al. 2016; Jiang et al. 2020), whereas Malat1 depletion from the brain was seen to impair fear extinction memory (Madugalle et al. 2023). These observations in diverse settings could all involve loss of the M1 peptide along with the RNA. We found that depletion of *Malat1* from neurons using either ASOs or shRNAs (data not shown) stimulated the expression of synaptic and other neuronal proteins. The varying observations made in different studies could arise from differences in cell types, culture systems, or methods of modulating *Malat1* levels and will need further investigation. In our system, the stimulated expression of synaptic proteins observed upon *Malat1* depletion appears to result at least in part from the loss of the M1 peptide.

The presence of *Malat1* as a translating mRNA in neurons also suggests a new possible source for physiological phenotypes observed in the *Malat1* knockout mice. These mice develop normally, and phenotypes from Malat1 loss have primarily been observed in either the nervous system or in cancer. It will be interesting to assess during the late neuroendocrine state of many cancers whether Malat1 becomes cytoplasmic and produces the M1 peptide. The role of micropeptides in these cellular processes will be an interesting area to explore.

Materials and methods

Tissue culture

We maintained mouse embryonic stem cells (E14) in ESC media containing DMEM (Fisher Scientific) supplemented with 15% ESC-qualified fetal bovine serum (FBS; Thermo Fisher Scientific), 1× nonessential amino acids (Thermo Fisher Scientific), 1× GlutaMAX (Thermo Fisher Scientific), 1× ESC-qualified nucleosides (EMD Millipore), 0.1 mM β-mercaptoethanol (Sigma-Aldrich), and 10^3 U/mL ESGRO leukemia inhibitor factor (LIF; EMD Millipore). N2a cells were maintained in Dulbecco's modified Eagle's medium (DMEM; Gibco, Invitrogen) supplemented with 10% FBS and penicillin–streptomycin. Cells were grown in incubator with 5% CO_2 at 37°C.

Primary cortical neuron culture

Embryonic day 16 C57BL/6J pregnant dams (Charles River Laboratories) were sacrificed by CO_2 overdose followed by cervical dislocation. Embryos were decapitated with sharp scissors, and cortices from males and females were dissected into ice-cold Hank's balanced salt solution (HBSS; Ca^{2+}- and Mg^{2+}- free) and randomly pooled. Cortices were treated with DNase1 and trypsin for 12 min in a 37°C water bath. Cortices were then washed once with HBSS and triturated in HBSS containing 10% DNase1 by pipetting up and down 12 times. Dissociated cells were spun down and washed once with plating media (neurobasal supplemented with 20% horse serum, 10% 250 mM sucrose in neurobasal, 0.25× GlutaMAX, 1× penicillin–streptomycin). Cortical neurons were plated at a density of ~500 cells/mm^2 for RNA or protein isolation or ~250 cells/mm^2 for

immunocytochemistry on tissue culture plates or coverslips (Fisher Scientific NC0672873) coated with 0.1 mg/mL poly-L-lysine (Sigma-Aldrich P1274-100mg) in borate buffer (0.1 M borate acid in H_2O at pH 8.5). Cells were initially plated in plating media and then refreshed with feeding media (neurobasal supplemented with B27, GlutaMAX) the second day after seeding. AraC was added at DIV4 to a final concentration of 2.5 μM. Half the culture media was replaced with fresh feeding media every 3 days beginning at DIV4. Primary cultures were maintained in a 37°C incubator supplemented with 5% CO_2.

GapmeR ASO knockdown

Cortical primary neurons were isolated from E16 embryos and plated at a density of ~250 cells/mm^2 on poly-L-lysine-coated plates or coverslips. GapmeR ASOs were gymnotically introduced into primary neurons at DIV8. GapmeRs were synthesized by IDT and transfected into cells as previously described (Williams et al. 2022). Briefly, for gymnotic delivery, the ASOs were added to the medium at the desired concentration (typically 2.5–5 μM) with a single treatment at DIV8. ASOs were not replenished with fresh medium additions. After 3 days of transfection, the cells were harvested for RNA extraction or immunofluorescence. The control and *Malat1* knockdown ASO sequences used were as follows: control-ASO (5′-/52MOErC/*/i2MOErC/*/i2MOErT/*/i2MOErT/*C*C*C*T*G*A*A*G*G*T*T*C*/i2MOErC/*/i2MOErT/*/i2MOErC/*/32MOErC/-3′), Malat1-ASO-a (5′-/52MOErG/*/i2MOErG/*/i2MOErG/*/i2MOErT/*/i2MOErC/*A*G*C*T*G*C*C*A*A*T*/i2MOErG/*/i2MOErC/*/i2MOErT/*/i2MOErA/*/32MOErG/-3′), Malat1-ASO-b (5′-/52MOErC/*/i2MOErC/*/i2MOErA/*/i2MOErG/*G*C*T*G*G*T*T*A*T*G*A*C*/i2MOErT/*/i2MOErC/*/i2MOErA/*/32MOErG/-3′), and Malat1-ASO-c (5′-/52MOErA/*/i2MOErA/*/i2MOErC/*/i2MOErT/*A*C*C*A*G*C*A*A*T*T*C*/i2MOErC/*/i2MOErG/*/i2MOErC/*/32MOErC/-3′).

Ribosome profiling

Primary cortical neurons were dissected from E16 embryos in C57BL/6 mice. The dissociated neurons were then plated on 10 cm dishes at a density of 2.25 million cells per dish. The primary neurons were cultured for 18 days. Cells were flash-frozen in liquid nitrogen at DIV18, moved to dry ice, and lysed in Turbo DNase I lysis buffer containing 100 μg/mL cycloheximide. Cell lysate was digested with RNase I at a ratio of 1 U of RNase:2 μg of RNA for 45 min on a nutator. The reaction was inhibited with Superase-In RNase inhibitor (Thermo Fisher Scientific AM 2696). Ribosome-protected fragments (RPFs) were pelleted through a sucrose cushion and centrifuged at 100,0000g for 2 h in a TLA centrifuge at 4°C. Ribosome-protected RNA fragments were recovered using the Zymo Direct RNA minipreparation kit. RNA was precipitated with isopropanol and resuspended in 10 mM Tris (pH 8). Footprint fragments were purified by gel electrophoresis on a 15% polyacrylamide TBE-urea gel stained with SYBR Gold. A 10 bp ladder, NI-800, and NEB miRNA were used as markers to select and isolate 17–34 nt fragments and ~28 nt footprints. RNA was extracted from gel slices overnight, precipitated with isopropanol, and resuspended in 10 mM Tris (pH 8). Footprints were then dephosphorylated and ligated to preadenylated 3′ linkers with unique barcodes. Ligation reactions were purified using the Zymo oligo Clean and Concentrator kits. Next, rRNA was depleted using a RiboZero Gold Illumina kit according to the manufacturer's protocol. Samples were again purified with the Clean and Concentrator kit. Reverse transcription was performed, cDNA was circularized using circligase II, and a library was constructed using PCR. Distribution analysis was conducted using HSD1000 screen tape and verified to be on average between 175 and 190 bp in length. Libraries were sequenced and aligned to the whole mouse genome. All steps were conducted using two biological replicates.

Immunofluorescence

ESCs, N2a cells, and cultured primary neuron cells were washed once with ice-cold PBSM (1× PBS, 5 mM $MgCl_2$), and then fixated with 4% paraformaldehyde in PBSM for 10 min at room temperature. After a 5 min wash with ice-cold PBSM, the cells were permeabilized with 0.3% Triton X-100 in PBSM for 7 min on ice. The cells were washed once with PBSM and blocked with 3% BSA (fraction V) in PBSM for 0.5 h at room temperature. The coverslips were then incubated with primary antibody in 3% BSA in PBSM for 1 h at room temperature. After three washes in PBST (1× PBS, 0.1% Tween 20), secondary antibody (goat antimouse-Cy3 [VWR- 95040-042], goat antirabbit cy5, or donkey antichicken 488) diluted in 1× PBS was added for 45 min at room temperature.

For IF only, cells were washed three times with PBST and then stained with DAPI in PBST for 15 min. Cells were mounted with Prolong mounting media overnight at room temperature. Antibodies used in this study were MAP2 (Abcam ab5392), STAU1 (Abcam ab73478), STAU2 (Thermo PA5-78473) Synaptophysin (sysy-101004), PSD95 (Antibodies Incorporated 75-028), GFP (Abcam ab290), Tuj1 (Abcam ab18207), M1 antibody generated from Thermo Scientific (project 1XJ0541), Vglut1 (Synaptic Systems 135 303), and Glur1 (Thermo MA5-27694).

For IF combined with RNA FISH, after three washes in 1× PBST, cells were refixed in 4% paraformaldehyde in PBSM for 10 min at room temperature. After a brief wash with PBSM, cells were equilibrated in 10% formamide in 2× SSC for 30 min. FISH probes were hybridized to cells at a concentration of 0.5 ng/μL in hybridization buffer (Biosearch SMF-HB1-10; 10% formamide added freshly) on parafilm and placed in a humidified box overnight. Cells were washed once with wash buffer A (Biosearch SMF-WA1-60) for 30 min at 37°C and then washed with wash buffer A containing 0.5 μg/mL DAPI for 30 min at 37°C. Cells were washed once with wash buffer B (Biosearch SMF-WB1-20) for 5 min at room temperature and mounted with Prolong antifade mounting media until completely dry. The slides were then used for confocal microscopy.

Competing interest statement

D.L.B. has equity in and serves on the board of directors for Panorama Medicine. This company did not contribute to or direct any of the research reported in this article.

Acknowledgments

We thank Dr. Prasanth Kannanganattu and Dr. David Spector for materials, and Dr. David Spector, Dr. Jennifer Achiro, Dr. Sylvia Newman, Dr. Kathrin Plath, and members of D.L.B.'s laboratory for helpful advice and suggestions. Technical support was provided by the University of California Los Angeles (UCLA) Neuroscience Genomics Core Sequencing Core and the California NanoSystems Institute (CNSI) Imaging Core at UCLA. This work was supported by National Institutes of Health grant R35GM136426, a research grant from the Broad Stem Cell Research Center at UCLA, and a research grant from the W.M. Keck Foundation to D.L.B.

Author contributions: W.X. and D.L.B. conceived the study and designed the experiments. W.X., R.H. and K.-H.Y. performed the experiments. M.N. acquired the experimental materials. C.-H.L. processed the sequencing data. W.X. and D.L.B. analyzed the experimental data. W.X. and D.L.B. wrote the manuscript, which was reviewed and edited by all of the authors.

References

Adam SA. 2016. Nuclear protein transport in digitonin permeabilized cells.*Methods Mol Biol* **1411:** 479–487. doi:10.1007/978-1-4939-3530-7_29

Alon S, Goodwin DR, Sinha A, Wassie AT, Chen F, Daugharthy ER, Bando Y, Kajita A, Xue AG, Marrett K, et al. 2021. Expansion sequencing: spatially precise in situ transcriptomics in intact biological systems. *Science* **371:** eaax2656. doi:10.1126/science.aax2656

Anderson DM, Anderson KM, Chang C-L, Makarewich CA, Nelson BR, McAnally JR, Kasaragod P, Shelton JM, Liou J, Bassel-Duby R, et al. 2015. A micropeptide encoded by a putative long noncoding RNA regulates muscle performance. *Cell* **160:** 595–606. doi:10.1016/j.cell.2015.01.009

Barczak W, Carr SM, Liu G, Munro S, Nicastri A, Lee LN, Hutchings C, Ternette N, Klenerman P, Kanapin A, et al. 2023. Long non-coding RNA-derived peptides are immunogenic and drive a potent anti-tumour response. *Nat Commun* **14:** 1078. doi:10.1038/s41467-023-36826-0

Batish M, Van Den Bogaard P, Kramer FR, Tyagi S. 2012. Neuronal mRNAs travel singly into dendrites. *Proc Natl Acad Sci* **109:** 4645–4650. doi:10.1073/pnas.1111226109

Bauer KE, De Queiroz BR, Kiebler MA, Besse F. 2023. RNA granules in neuronal plasticity and disease. *Trends Neurosci* **46:** 525–538. doi:10.1016/j.tins.2023.04.004

Berg MG, Singh LN, Younis I, Liu Q, Pinto AM, Kaida D, Zhang Z, Cho S, Sherrill-Mix S, Wan L, et al. 2012. U1 snRNP determines mRNA length and regulates isoform expression. *Cell* **150:** 53–64. doi:10.1016/j.cell.2012.05.029

Bergmann JH, Spector DL. 2014. Long non-coding RNAs: modulators of nuclear structure and function. *Curr Opin Cell Biol* **26:** 10–18. doi:10.1016/j.ceb.2013.08.005

Bernard D, Prasanth KV, Tripathi V, Colasse S, Nakamura T, Xuan Z, Zhang MQ, Sedel F, Jourdren L, Coulpier F, et al. 2010. A long nuclear-retained non-coding RNA regulates synaptogenesis by modulating gene expression. *EMBO J* **29:** 3082–3093. doi:10.1038/emboj.2010.199

Bi J, Tsai N-P, Lin Y-P, Loh HH, Wei L-N. 2006. Axonal mRNA transport and localized translational regulation of κ-opioid receptor in primary neurons of dorsal root ganglia. *Proc Natl Acad Sci* **103:** 19919–19924. doi:10.1073/pnas.0607394104

Bi P, Ramirez-Martinez A, Li H, Cannavino J, McAnally JR, Shelton JM, Sánchez-Ortiz E, Bassel-Duby R, Olson EN. 2017. Control of muscle formation by the fusogenic micropeptide myomixer. *Science* **356:** 323–327. doi:10.1126/science.aam9361

Böhmdorfer G, Wierzbicki AT. 2015. Control of chromatin structure by long noncoding RNA. *Trends Cell Biol* **25:** 623–632. doi:10.1016/j.tcb.2015.07.002

Brar GA, Yassour M, Friedman N, Regev A, Ingolia NT, Weissman JS. 2012. High-resolution view of the yeast meiotic program revealed by ribosome profiling. *Science* **335:** 552–557. doi:10.1126/science.1215110

Brown JA, Valenstein ML, Yario TA, Tycowski KT, Steitz JA. 2012. Formation of triple-helical structures by the 3′-end sequences of MALAT1 and MENβ noncoding RNAs. *Proc Natl Acad Sci* **109:** 19202–19207. doi:10.1073/pnas.1217338109

Buxbaum AR, Wu B, Singer RH. 2014. Single β-actin mRNA detection in neurons reveals a mechanism for regulating its translatability. *Science* **343:** 419–422. doi:10.1126/science.1242939

Chen L, Feng P, Zhu X, He S, Duan J, Zhou D. 2016. Long noncoding RNA Malat1 promotes neurite outgrowth through activation of ERK/MAPK signalling pathway in N2a cells. *J Cell Mol Med* **20:** 2102–2110. doi:10.1111/jcmm.12904

Chen X, He L, Zhao Y, Li Y, Zhang S, Sun K, So K, Chen F, Zhou L, Lu L, et al. 2017. Malat1 regulates myogenic differentiation and muscle regeneration through modulating MyoD transcriptional activity. *Cell Discov* **3:** 17002. doi:10.1038/celldisc.2017.2

Conrad NK, Steitz JA. 2005. A Kaposi's sarcoma virus RNA element that increases the nuclear abundance of intronless transcripts. *EMBO J* **24:** 1831–1841. doi:10.1038/sj.emboj.7600662

Duffy EE, Finander B, Choi G, Carter AC, Pritisanac I, Alam A, Luria V, Karger A, Phu W, Sherman MA, et al. 2022. Developmental dynamics of RNA translation in the human brain. *Nat Neurosci* **25:** 1353–1365. doi:10.1038/s41593-022-01164-9

Engreitz JM, Sirokman K, McDonel P, Shishkin AA, Surka C, Russell P, Grossman SR, Chow AY, Guttman M, Lander ES. 2014. RNA–RNA interactions enable specific targeting of noncoding RNAs to nascent pre-mRNAs and chromatin sites. *Cell* **159:** 188–199. doi:10.1016/j.cell.2014.08.018

Formicola N, Heim M, Dufourt J, Lancelot A-S, Nakamura A, Lagha M, Besse F. 2021. Tyramine induces dynamic RNP granule remodeling and translation activation in the *Drosophila* brain. *Elife* **10:** e65742. doi:10.7554/eLife.65742

Fritzsche R, Karra D, Bennett KL, Ang FY, Heraud-Farlow JE, Tolino M, Doyle M, Bauer KE, Thomas S, Planyavsky M, et al. 2013. Interactome of two diverse RNA granules links mRNA localization to translational repression in neurons. *Cell Rep* **5:** 1749–1762. doi:10.1016/j.celrep.2013.11.023

Grzejda D, Mach J, Schweizer JA, Hummel B, Rezansoff AM, Eggenhofer F, Panhale A, Lalioti M-E, Cabezas Wallscheid N, Backofen R, et al. 2022. The long noncoding RNA *mimi* scaffolds neuronal granules to maintain nervous system maturity. *Sci Adv* **8:** eabo5578. doi:10.1126/sciadv.abo5578

Holt CE, Martin KC, Schuman EM. 2019. Local translation in neurons: visualization and function. *Nat Struct Mol Biol* **26:** 557–566. doi:10.1038/s41594-019-0263-5

Huang J-Z, Chen M, Chen D, Gao X-C, Zhu S, Huang H, Hu M, Zhu H, Yan G-R. 2017. A peptide encoded by a putative lncRNA HOXB-AS3 suppresses colon cancer growth. *Mol Cell* **68:** 171–184.e6. doi:10.1016/j.molcel.2017.09.015

Ingolia NT, Brar GA, Stern-Ginossar N, Harris MS, Talhouarne GJS, Jackson SE, Wills MR, Weissman JS. 2014. Ribosome profiling reveals pervasive translation outside of annotated protein-coding genes. *Cell Rep* **8:** 1365–1379. doi:10.1016/j.celrep.2014.07.045

Jiang T, Cai Z, Ji Z, Zou J, Liang Z, Zhang G, Liang Y, Lin H, Tan M. 2020. The lncRNA MALAT1/miR-30/spastin axis regulates hippocampal neurite outgrowth. *Front Cell Neurosci* **14:** 555747. doi:10.3389/fncel.2020.555747

Karakas D, Ozpolat B. 2021. The role of LncRNAs in translation. *RNA* **7:** 16. doi:10.3390/ncrna7010016

Khanduja JS, Calvo IA, Joh RI, Hill IT, Motamedi M. 2016. Nuclear noncoding RNAs and genome stability. *Mol Cell* **63:** 7–20. doi:10.1016/j.molcel.2016.06.011

Kiebler MA, Bassell GJ. 2006. Neuronal RNA granules: movers and makers. *Neuron* **51:** 685–690. doi:10.1016/j.neuron.2006.08.021

Kim J, Piao H-L, Kim B-J, Yao F, Han Z, Wang Y, Xiao Z, Siverly AN, Lawhon SE, Ton BN, et al. 2018. Long noncoding RNA MALAT1 suppresses breast cancer metastasis. *Nat Genet* **50:** 1705–1715. doi:10.1038/s41588-018-0252-3

Knowles RB, Sabry JH, Martone ME, Deerinck TJ, Ellisman MH, Bassell GJ, Kosik KS. 1996. Translocation of RNA granules in living neurons. *J Neurosci* **16:** 7812–7820. doi:10.1523/JNEUROSCI.16-24-07812.1996

Krichevsky AM, Kosik KS. 2001. Neuronal RNA granules. *Neuron* **32:** 683–696. doi:10.1016/S0896-6273(01)00508-6

Lee S, Kopp F, Chang T-C, Sataluri A, Chen B, Sivakumar S, Yu H, Xie Y, Mendell JT. 2016. Noncoding RNA NORAD regulates genomic stability by sequestering PUMILIO proteins. *Cell* **164:** 69–80. doi:10.1016/j.cell.2015.12.017

Madugalle SU, Liau W-S, Zhao Q, Li X, Gong H, Marshall PR, Periyakaruppiah A, Zajaczkowski EL, Leighton LJ, Ren H, et al. 2023. Synapse-enriched m^6A-modified Malat1 interacts with the novel m^6A reader, DPYSL2, and is required for fear-extinction memory. *J Neurosci* **43:** 7084–7100. doi:10.1523/JNEUROSCI.0943-23.2023

Mallardo M, Deitinghoff A, Müller J, Goetze B, Macchi P, Peters C, Kiebler MA. 2003. Isolation and characterization of Staufen-containing ribonucleoprotein particles from rat brain. *Proc Natl Acad Sci* **100:** 2100–2105. doi:10.1073/pnas.0334355100

Matsumoto A, Pasut A, Matsumoto M, Yamashita R, Fung J, Monteleone E, Saghatelian A, Nakayama KI, Clohessy JG, Pandolfi PP. 2017. mTORC1 and muscle regeneration are regulated by the LINC00961-encoded SPAR polypeptide. *Nature* **541:** 228–232. doi:10.1038/nature21034

Mattick JS, Amaral PP, Carninci P, Carpenter S, Chang HY, Chen L-L, Chen R, Dean C, Dinger ME, Fitzgerald KA, et al. 2023. Long non-coding RNAs: definitions, functions, challenges and recommendations. *Nat Rev Mol Cell Biol* **24:** 430–447. doi:10.1038/s41580-022-00566-8

Miao H, Wu F, Li Y, Qin C, Zhao Y, Xie M, Dai H, Yao H, Cai H, Wang Q, et al. 2022. MALAT1 modulates alternative splicing by cooperating with the splicing factors PTBP1 and PSF. *Sci Adv* **8:** eabq7289. doi:10.1126/sciadv.abq7289

Miyagawa R, Tano K, Mizuno R, Nakamura Y, Ijiri K, Rakwal R, Shibato J, Masuo Y, Mayeda A, Hirose T, et al. 2012. Identification of *cis*- and *trans*-acting factors involved in the localization of MALAT-1 noncoding RNA to nuclear speckles. *RNA* **18:** 738–751. doi:10.1261/rna.028639.111

Mofatteh M. 2020. mRNA localization and local translation in neurons. *AIMS Neurosci* **7:** 299–310. doi:10.3934/Neuroscience.2020016

Munschauer M, Nguyen CT, Sirokman K, Hartigan CR, Hogstrom L, Engreitz JM, Ulirsch JC, Fulco CP, Subramanian V, Chen J, et al. 2018. The NORAD lncRNA assembles a topoisomerase complex critical for genome stability. *Nature* **561:** 132–136. doi:10.1038/s41586-018-0453-z

Nakagawa S, Ip JY, Shioi G, Tripathi V, Zong X, Hirose T, Prasanth KV. 2012. Malat1 is not an essential component of nuclear speckles in mice. *RNA* **18:** 1487–1499. doi:10.1261/rna.033217.112

Nelson BR, Makarewich CA, Anderson DM, Winders BR, Troupes CD, Wu F, Reese AL, McAnally JR, Chen X, Kavalali ET, et al. 2016. A peptide encoded by a transcript annotated as long noncoding RNA enhances SERCA activity in muscle. *Science* **351:** 271–275. doi:10.1126/science.aad4076

Niklas J, Melnyk A, Yuan Y, Heinzle E. 2011. Selective permeabilization for the high-throughput measurement of compartmented enzyme activities in mammalian cells. *Anal Biochem* **416:** 218–227. doi:10.1016/j.ab.2011.05.039

Noh JH, Kim KM, McClusky WG, Abdelmohsen K, Gorospe M. 2018. Cytoplasmic functions of long noncoding RNAs. *WIREs RNA* **9:** e1471. doi:10.1002/wrna.1471

Ouyang J, Zhong Y, Zhang Y, Yang L, Wu P, Hou X, Xiong F, Li X, Zhang S, Gong Z, et al. 2022. Long non-coding RNAs are involved in alternative splicing and promote cancer progression. *Br J Cancer* **126:** 1113–1124. doi:10.1038/s41416-021-01600-w

Powers EN, Chan C, Doron-Mandel E, Llacsahuanga Allcca L, Kim Kim J, Jovanovic M, Brar GA. 2022. Bidirectional promoter activity from expression cassettes can drive off-target repression of neighboring gene translation. *Elife* **11:** e81086. doi:10.7554/eLife.81086

Ransohoff JD, Wei Y, Khavari PA. 2018. The functions and unique features of long intergenic non-coding RNA. *Nat Rev Mol Cell Biol* **19:** 143–157. doi:10.1038/nrm.2017.104

Ruiz-Orera J, Messeguer X, Subirana JA, Alba MM. 2014. Long non-coding RNAs as a source of new peptides. *Elife* **3:** e03523. doi:10.7554/eLife.03523

Saini H, Bicknell AA, Eddy SR, Moore MJ. 2019. Free circular introns with an unusual branchpoint in neuronal projections. *Elife* **8:** e47809. doi:10.7554/eLife.47809

Sato K, Sakai M, Ishii A, Maehata K, Takada Y, Yasuda K, Kotani T. 2022. Identification of embryonic RNA granules that act as sites of mRNA translation after changing their physical properties. *iScience* **25:** 104344. doi:10.1016/j.isci.2022.104344

Schuman EM. 1999. mRNA trafficking and local protein synthesis at the synapse. *Neuron* **23:** 645–648. doi:10.1016/S0896-6273(01)80023-4

Sharangdhar T, Sugimoto Y, Heraud-Farlow J, Fernández-Moya SM, Ehses J, Ruiz De Los Mozos I, Ule J, Kiebler MA. 2017. A retained intron in the 3′-UTR of *Calm3* mRNA mediates its Staufen2- and activity-dependent localization to neuronal dendrites. *EMBO Rep* **18:** 1762–1774. doi:10.15252/embr.201744334

Shih C-H, Chuang L-L, Tsai M-H, Chen L-H, Chuang EY, Lu T-P, Lai L-C. 2021. Hypoxia-induced MALAT1 promotes the proliferation and migration of breast cancer cells by sponging MiR-3064-5p. *Front Oncol* **11:** 658151. doi:10.3389/fonc.2021.658151

Sun Y, Wang T, Lv Y, Li J, Jiang X, Jiang J, Zhang D, Bian W, Zhang C. 2023. MALAT1 promotes platelet activity and thrombus

formation through PI3k/Akt/GSK-3β signalling pathway. *Stroke Vasc Neurol* **8:** 181–192. doi:10.1136/svn-2022-001498

Tang Y, Wang J, Lian Y, Fan C, Zhang P, Wu Y, Li X, Xiong F, Li X, Li G, et al. 2017. Linking long non-coding RNAs and SWI/SNF complexes to chromatin remodeling in cancer. *Mol Cancer* **16:** 42. doi:10.1186/s12943-017-0612-0

Tripathi V, Ellis JD, Shen Z, Song DY, Pan Q, Watt AT, Freier SM, Bennett CF, Sharma A, Bubulya PA, et al. 2010. The nuclear-retained noncoding RNA MALAT1 regulates alternative splicing by modulating SR splicing factor phosphorylation. *Mol Cell* **39:** 925–938. doi:10.1016/j.molcel.2010.08.011

Ueda HH, Nagasawa Y, Sato A, Onda M, Murakoshi H. 2022. Chronic neuronal excitation leads to dual metaplasticity in the signaling for structural long-term potentiation. *Cell Rep* **38:** 110153. doi:10.1016/j.celrep.2021.110153

Venters CC, Oh J-M, Di C, So BR, Dreyfuss G. 2019. U1 snRNP telescripting: suppression of premature transcription termination in introns as a new layer of gene regulation. *Cold Spring Harb Perspect Biol* **11:** a032235. doi:10.1101/cshperspect.a032235

Wang H, Wang Y, Xie S, Liu Y, Xie Z. 2016. Global and cell-type specific properties of lincRNAs with ribosome occupancy. *Nucleic Acids Res gkw* **909:** gkw909. doi:10.1093/nar/gkw909

Wang C, Lu T, Emanuel G, Babcock HP, Zhuang X. 2019. Imaging-based pooled CRISPR screening reveals regulators of lncRNA localization. *Proc Natl Acad Sci USA* **116:** 10842–10851. doi:10.1073/pnas.1903808116

Williams LA, Gerber DJ, Elder A, Tseng WC, Baru V, Delaney-Busch N, Ambrosi C, Mahimkar G, Joshi V, Shah H, et al. 2022. Developing antisense oligonucleotides for a TECPR2 mutation-induced, ultra-rare neurological disorder using patient-derived cellular models. *Mol Ther Nucleic Acids* **29:** 189–203. doi:10.1016/j.omtn.2022.06.015

Wilusz JE, Freier SM, Spector DL. 2008. 3′ end processing of a long nuclear-retained noncoding RNA yields a tRNA-like cytoplasmic RNA. *Cell* **135:** 919–932. doi:10.1016/j.cell.2008.10.012

Wilusz JE, JnBaptiste CK, Lu LY, Kuhn C-D, Joshua-Tor L, Sharp PA. 2012. A triple helix stabilizes the 3′ ends of long noncoding RNAs that lack poly(A) tails. *Genes Dev* **26:** 2392–2407. doi:10.1101/gad.204438.112

Xiao W, Yeom K-H, Lin C-H, Black DL. 2023. Improved enzymatic labeling of fluorescent in situ hybridization probes applied to the visualization of retained introns in cells. *RNA* **29:** 1274–1287. doi:10.1261/rna.079591.123

Xie S-J, Diao L-T, Cai N, Zhang L-T, Xiang S, Jia C-C, Qiu D-B, Liu C, Sun Y-J, Lei H, et al. 2021. mascRNA and its parent lncRNA MALAT1 promote proliferation and metastasis of hepatocellular carcinoma cells by activating ERK/MAPK signaling pathway. *Cell Death Discov* **7:** 110. doi:10.1038/s41420-021-00497-x

Xing J, Liu H, Jiang W, Wang L. 2021. LncRNA-encoded peptide: functions and predicting methods. *Front Oncol* **10:** 622294. doi:10.3389/fonc.2020.622294

Yeom K-H, Pan Z, Lin C-H, Lim HY, Xiao W, Xing Y, Black DL. 2021. Tracking pre-mRNA maturation across subcellular compartments identifies developmental gene regulation through intron retention and nuclear anchoring. *Genome Res* **31:** 1106–1119. doi:10.1101/gr.273904.120

Yin Y, Lu JY, Zhang X, Shao W, Xu Y, Li P, Hong Y, Cui L, Shan G, Tian B, et al. 2020. U1 snRNP regulates chromatin retention of noncoding RNAs. *Nature* **580:** 147–150. doi:10.1038/s41586-020-2105-3

Young AP, Jackson DJ, Wyeth RC. 2020. A technical review and guide to RNA fluorescence in situ hybridization. *PeerJ* **8:** e8806. doi:10.7717/peerj.8806

Zhang Q, Vashisht AA, O'Rourke J, Corbel SY, Moran R, Romero A, Miraglia L, Zhang J, Durrant E, Schmedt C, et al. 2017. The microprotein minion controls cell fusion and muscle formation. *Nat Commun* **8:** 15664. doi:10.1038/ncomms15664

Zhang C, Zhou B, Gu F, Liu H, Wu H, Yao F, Zheng H, Fu H, Chong W, Cai S, et al. 2022. Micropeptide PACMP inhibition elicits synthetic lethal effects by decreasing CtIP and poly(ADP-ribosyl)ation. *Mol Cell* **82:** 1297–1312.e8. doi:10.1016/j.molcel.2022.01.020

Zhao Y, Zhou L, Li H, Sun T, Wen X, Li X, Meng Y, Li Y, Liu M, Liu S, et al. 2021. Nuclear-encoded lncRNA MALAT1 epigenetically controls metabolic reprogramming in HCC cells through the mitophagy pathway. *Mol Ther Nucleic Acids* **23:** 264–276. doi:10.1016/j.omtn.2020.09.040

Zhu N, Ahmed M, Li Y, Liao JC, Wong PK. 2023. Long noncoding RNA MALAT1 is dynamically regulated in leader cells during collective cancer invasion. *Proc Natl Acad Sci* **120:** e2305410120. doi:10.1073/pnas.2305410120